

Rational Design of Selective Submicromolar Inhibitors of *Tritrichomonas foetus* Hypoxanthine-Guanine-Xanthine Phosphoribosyltransferase[†]

Alex M. Aronov, Narsimha R. Munagala, Paul R. Ortiz de Montellano, Irwin D. Kuntz, and Ching C. Wang*

Department of Pharmaceutical Chemistry, University of California, San Francisco, California 94143-0446

Received November 4, 1999; Revised Manuscript Received January 6, 2000

ABSTRACT: All parasitic protozoa lack the ability to synthesize purine nucleotides de novo, relying instead on purine salvage enzymes for their survival. Hypoxanthine-guanine-xanthine phosphoribosyltransferase (HGXPRT) from the protozoan parasite *Tritrichomonas foetus* is a rational target for antiparasitic drug design because it is the primary enzyme the parasite uses to salvage purine bases from the host. The study presented here is a continuation of our efforts to use the X-ray structure of the *T. foetus* HGXPRT–GMP complex to design compounds that bind tightly to the purine pocket of HGXPRT. The goal of the current project was to improve the affinity and selectivity of previously identified HGXPRT inhibitor **TF1** [4-(3-nitroanilino)phthalic anhydride]. A virtual library of substituted 4-phthalimidocarboxanilides was constructed using methods of structure-based drug design, and was implemented synthetically on solid support. Compound **20** [(4'-phthalimido)carboxamido-3-benzyloxybenzene] was then used as a secondary lead for the second round of combinatorial chemistry, producing a number of low-micromolar inhibitors of HGXPRT. One of these compounds, **TF2** [(4'-phthalimido)carboxamido-3-(4-bromobenzyloxy)benzene], was further characterized as a competitive inhibitor of *T. foetus* HGXPRT with respect to guanine with a K_i of 0.49 μM and a 30-fold selectivity over the human HGPRT. **TF2** inhibited the growth of cultured *T. foetus* cells in a concentration-dependent manner with an ED_{50} of 2.8 μM , and this inhibitory effect could be reversed by addition of exogenous hypoxanthine. These studies underscore the efficiency of combining structure-based drug design with combinatorial chemistry to produce effective species-specific enzyme inhibitors of medicinal importance.

Rapid growth in the field of parasite structural biology, spurred by recent advances in parasite biology and biochemistry, is becoming increasingly important in the process of drug discovery for parasitic infections (1). A combination of rational target selection and molecular modeling tools, aided by new combinatorial chemistry technologies, appears to have become a method of choice for designing potent and selective ligands for a number of targets in parasites (2, 3).

All protozoan parasites lack the ability to synthesize purine nucleotides de novo. Instead, they utilize purine salvage pathways to convert the host organism's purine bases and nucleosides to the corresponding nucleotides (4). Purine phosphoribosyltransferases (PRTs)¹ are a class of enzymes that catalyze the reaction of a purine with α -D-5-phosphoribosyl-1-pyrophosphate (PRPP) to produce nucleoside monophosphates via nucleophilic displacement of pyrophosphate. Inhibiting PRTs could represent an efficient approach to antiparasite chemotherapy (4, 5).

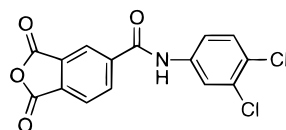
Tritrichomonas foetus, an anaerobic flagellated protozoan that causes urogenital trichomoniasis in cattle, relies primarily

on a single enzyme, hypoxanthine-guanine-xanthine phosphoribosyltransferase (HGXPRT), to replenish its purine nucleotide pool (6). The X-ray structure of this enzyme is available (7), and it was used in a search for novel scaffolds that could be used to design new selective inhibitors of HGXPRT. The DOCK program suite (8–11) was used by Somoza et al. to screen the Available Chemicals Directory (12) (ACD) for potential HGXPRT inhibitors (13). Isatin and phthalic anhydride were identified as two novel scaffolds capable of mimicking the substrate purine base and acting as competitive inhibitors of the target enzyme. **TF1** [4-(3-nitroanilino)phthalic anhydride], a phthalic anhydride derivative, was shown to be effective in killing the cultured parasites; the ED_{50} value for this compound when tested in parasite culture was essentially identical with the in vitro IC_{50} against *T. foetus* HGXPRT (50 μM), and parasite growth inhibition could be reversed by addition of the natural substrate hypoxanthine to the culture medium (13).

[†] This work was supported by the National Institutes of Health (Grant AI-19319 to C.C.W., Grant GM31497 to I.D.K., and Grant GM56531 to P.R.O.d.M.).

* To whom correspondence should be addressed: Department of Pharmaceutical Chemistry, 513 Parnassus Ave., Box 0446, University of California, San Francisco, CA 94143-0446. Telephone: (415) 476-1321. Fax: (415) 476-3382. E-mail: ccwang@cgl.ucsf.edu.

¹ Abbreviations: ACD, Available Chemicals Directory; CGI, Common Gateway Interface; DIPEA, diisopropylethylamine; HGPRT, hypoxanthine-guanine phosphoribosyltransferase; HGXPRT, hypoxanthine-guanine-xanthine phosphoribosyltransferase; HPLC, high-performance liquid chromatography; GMP, guanosine 5'-monophosphate; GPRT, guanine phosphoribosyltransferase; PRPP, α -D-5-phosphoribosyl 1-pyrophosphate; PRT, phosphoribosyltransferase; PyBOP, benzotriazol-1-yl-oxy-tris-pyrrolidino-phosphonium hexafluorophosphate; PyBrOP, bromo-tris-pyrrolidino-phosphonium hexafluorophosphate; SMILES, Simplified Molecular Input Line Entry System; TFA, trifluoroacetic acid; TLC, thin-layer chromatography.



TF1

Despite having the necessary enzymatic machinery for de novo purine production, mammals also utilize purine salvage pathways. The sequence of HGPRT, the mammalian counterpart of HGXPRT, is 27% identical with that of the tritrichomonal enzyme (14). A decrease in human HGPRT activity has been demonstrated to be responsible for gouty arthritis and the Lesch-Nyhan syndrome. Therefore, the compounds being developed as *T. foetus* HGXPRT inhibitors should not interfere with mammalian HGPRT activity. **TF1** fulfills this requirement; it has been shown to be more than 20-fold selective for the parasite HGXPRT over the human HGPRT (13).

Two major problems associated with practical use of **TF1** were (i) the relatively low potency and (ii) its possible promiscuity as a nonselective acylating agent, which could not only lead to serious side effects, but would also drastically decrease the agent's bioavailability. Herein, we report on the utility of molecular docking in conjunction with molecular similarity and diversity approaches to facilitate iterative combinatorial library generation, leading to the discovery of selective submicromolar inhibitors of *T. foetus* HGXPRT.

MATERIALS AND METHODS

Materials. Trityl chloride resin and PyBrOP were purchased from Novabiochem (San Diego, CA). All anhydrous solvents were obtained from Aldrich (Milwaukee, WI). TLC was carried out with precoated silica gel F₂₅₄ plates from Analtech (Newark, DE), and spots were detected under UV light (254 nm). Ninhydrin staining was used for detection of amines. Flash chromatography was carried out with silica gel (230–400 mesh, Merck). The UV source used for photochemical brominations was a Spectroline ENF-280C lamp (17 W) from Spectronics Corp. (Westbury, NY). NMR spectra were recorded on Varian (Palo Alto, CA) Inova 400 and Varian Inova 600 spectrometers. Key target compounds were purified by reverse phase HPLC on a C₁₈ column from Alltech (Deerfield, IL) with a MeOH/H₂O elution gradient. The purity was confirmed by using a C₄ column from Vydac (Hesperia, CA). The HPLC interface consisted of Rainin HPXL solvent delivery modules and a Rainin Dynamax UV-1 UV–vis spectrophotometric detector with UV detection at 254 nm. HPLC solvents were of the highest grade commercially available and were used as received.

Structure Analysis. The crystal structure of *T. foetus* HGXPRT (1hgx) was determined by Somoza et al. (7), and the crystal structure of the human HGPRT (1hmp) was determined by Eads et al. (15). The software packages Sybyl (16) and Insight II (17) were used for display and analysis of the structures.

Database Mining. UC_Select (18) in combination with the Daylight version of ACD was used to identify original reagent sets, as well as for the elimination of reagents that had unattractive chemical or pharmaceutical properties. UC_React (18) interfaced with Sybyl's CONCORD module (16) was used to build the virtual library for docking.

Similarity and superstructure searches of the ACD were performed with Daylight's Merlin system (19), using a Tanimoto similarity metric and Daylight's hashed connectivity fingerprints.

Docking. DOCK4.01 (11) was used to screen the virtual phthalimide library to limit the size of the primary library. A typical docking process involves (a) creating a negative image of the active site using sphere sets, (b) matching existing sphere sets to molecules in the library, (c) scoring and ranking compounds on the basis of goodness of fit, and (d) reviewing the conformations of the best-scoring compounds. The approach taken in this study differed from the general method in the following aspects: (a) xanthine was mapped onto the guanine moiety of GMP, and the 6-oxo and 1-NH of xanthine were matched to the O=C–NH–C=O portion of phthalimide; to facilitate correct matching, spheres at positions C1 and C3 in the benzene ring of phthalimide were removed from the sphere set, and the sphere for C2 was specified for chemical matching; (b) in every case, preorientation of the library with the sphere set (orientation search without scoring) followed by rigid docking of the preoriented library (orientation search with scoring for rigid molecules) and subsequent flexible scoring (scoring of a variety of conformations for selected orientations) gave the best results. In modeling substituents in the aniline ring of **20**, we used the DOCK-derived conformation for **20** as a starting point for flexible docking.

Enzyme Assays. Isolation (14, 20) and assays (21) of *T. foetus* HGXPRT and human HGPRT were performed as described previously. The substrates were present at the following concentrations: 20 μ M guanine ($K_M = 2.4 \mu$ M) and 1 mM PRPP ($K_M = 45 \mu$ M). The compounds that were tested were dissolved in DMSO-*d*₆, and concentrations were determined by integration of NMR peaks with methylene chloride as an internal standard. The concentration of DMSO in the assays was kept at 10%.

Cell Culture Assays. *T. foetus* strain kv1 trophozoites were cultivated in Diamond's TYM medium at 37 °C. Cell densities in time samples were determined using a hemocytometer. The concentration of DMSO in culture medium was maintained at or below 1%, which had no apparent effect on cell growth.

Synthesis. 4-Carboxyphthalimide. The title compound was obtained by melting trimellitic anhydride with ammonium carbonate at 280 °C as described previously (22): ¹H NMR (DMSO-*d*₆) δ 7.93 (d, 1, H6), 8.07 (s, 1, H3), 8.14 (d, 1, H5).

N-Trityl-4-carboxyphthalimide Resin. To trityl chloride resin (5 g, 10.25 mmol, 200–400 mesh, 1% divinylbenzene-cross-linked polystyrene) presoaked in 80 mL of dry acetonitrile for 30 min were added 5 g (26 mmol) of 4-carboxyphthalimide and 6 mL (34 mmol) of diisopropylethylamine, and the suspension was refluxed for 72 h. Following filtration, the polymer was washed with 300 mL of dimethylformamide and then 300 mL of CH₂Cl₂. The loading was determined by weight difference, and confirmed to be 0.5 mmol/g of resin by TFA-induced cleavage of 4-carboxyphthalimide from the resin.

Aniline Coupling/Product Cleavage Procedure. To 100 mg of resin (0.06 mmol of 4-carboxyphthalimide) presoaked in 2 mL of dimethylacetamide for 30 min were added 0.56 g (20 equiv) of PyBrOP, 0.52 mL (50 equiv) of diisopro-

pylethylamine, and 1.2 mmol (20 equiv) of the desired aniline. The suspension was shaken for 5 days at 37 °C, followed by filtration to remove excess reagents. The resin was washed with 5 mL of dimethylformamide, 5 mL of ethyl acetate, 5 mL of methanol, and 10 mL of CH₂Cl₂, and was then air-dried. To facilitate cleavage of the target compounds, the resin was suspended in 2 mL of TFA for 4 h. The resin was removed by filtration; the resulting filtrate was dried in vacuo, and the product was loaded onto a short plug of silica gel. Quick elution with ethyl acetate allowed for removal of colored impurities undesirable in a spectrophotometric assay.

3-Methyl-5-nitrobenzyl Bromide. To a solution of 0.8 g (5.3 mmol) of *m*-nitroxyline in 10 mL of CCl₄ was added 1.23 g (6.9 mmol, 1.3 equiv) of *N*-bromosuccinimide, and the mixture was irradiated with a UV source at reflux for 4 h. The resulting mixture was dried in vacuo, suspended in hexane, and filtered. The filtrate was dried to afford a 10:1:3 mixture of monobromide, starting material, and dibromide. The title material was purified in 65% yield by silica gel chromatography using a 0 to 5% ethyl acetate/hexane gradient: ¹H NMR (CDCl₃) δ 2.46 (s, 3, CH₃), 4.48 (s, 2, CH₂), 7.52 (s, 1, H₂), 7.97 (s, 1, H₄), 8.05 (s, 1, H₆).

3-Methyl-5-(phenoxymethyl)nitrobenzene. 3-Methyl-5-nitrobenzyl bromide (0.8 g, 3.5 mmol) was dissolved in 10 mL of DMSO. To the mixture were added 0.46 g (4.9 mmol, 1.4 equiv) of phenol and 300 mg (5.3 mmol) of potassium hydroxide, and the solution was stirred for 2 h, until essentially all the potassium hydroxide dissolved. The reactants were diluted into 30 mL of ethyl acetate, and washed twice with an equal volume of water. The organic layer was dried with sodium sulfate, and the solvent was removed in vacuo. Silica gel purification (in hexane, followed by a 0 to 5% ethyl acetate/hexane gradient) afforded the title product (0.81 g, 95% yield): ¹H NMR (CDCl₃) δ 2.49 (s, 3, CH₃), 5.11 (s, 2, CH₂), 6.95–7.03 (m, 3, phenolic H_p and 2 H_m), 7.24–7.34 (m, 2, phenolic 2 H_o), 7.58 (s, 1, H₂), 7.99 (s, 1, H₆), 8.11 (s, 1, H₄).

3-Methyl-5-(phenoxymethyl)aniline. To a solution of 0.81 g (3.3 mmol) of (3-methyl-5-phenoxymethyl)nitrobenzene in 10 mL of methanol was added 30 mg of Pd/C catalyst, and the mixture was shaken under H₂ for 2 h (35 psi). The resulting solution was filtered through Celite, and the solvent was removed in vacuo. The title product was purified on alumina gel (hexane/ethyl acetate) to homogeneity (0.64 g, 90% yield): ¹H NMR (CDCl₃) δ 2.25 (s, 3, CH₃), 4.92 (s, 2, CH₂), 6.4–6.7 (3s, 3, H₂, H₄, H₆), 6.95–6.97 (m, 3, phenolic H_p and 2 H_m), 7.20–7.28 (m, 2, phenolic 2 H_o).

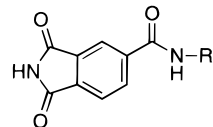
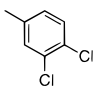
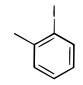
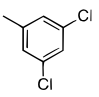
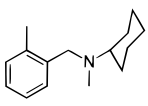
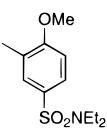
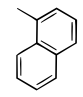
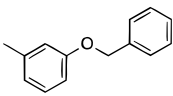
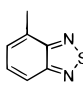
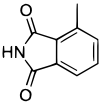
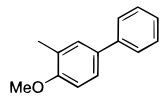
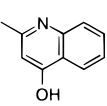
3-(Benzyloxy)-6-chloronitrobenzene: ¹H NMR (CDCl₃) δ 5.10 (s, 2, CH₂), 7.11 (dd, 1, H₄), 7.38–7.43 (m, 6, phenyl and H₅), 7.46 (d, 1, H₂).

(4'-Phthalimidocarboxamido)-3,4-dichlorobenzene (1): ¹H NMR (DMSO-*d*₆) δ 7.61 (d, 1, H₆), 7.75 (dd, 1, H₅), 7.95 (d, 1, H_{6'}), 8.14 (d, 1, H₂), 8.32 (d, 1, H_{5'}), 8.35 (s, 1, H_{3'}).

(4'-Phthalimidocarboxamido)-3-methyl-5-(phenoxymethyl)benzene (20a): ¹H NMR (DMSO-*d*₆) δ 2.30 (s, 3, CH₃), 5.04 (s, 2, CH₂), 6.90–7.05 (m, 4, phenyl H_p + 2H_o, H₄), 7.24–7.30 (m, 2, 2H_m), 7.56, 7.65 (2s, 2, H₂, H₆), 7.93 (d, 1, H_{6'}), 8.32 (d, 1, H_{5'}), 8.33 (s, 1, H_{3'}).

(4'-Phthalimidocarboxamido)-3-(benzyloxy)-6-chlorobenzene (20b): ¹H NMR (DMSO-*d*₆) δ 5.11 (s, 2, CH₂), 6.97 (dd, 1, H₄), 7.28 (d, 1, H₂), 7.31–7.46 (m, 6, phenyl,

Table 1: Inhibition of *T. foetus* HGXPRT (IC₅₀) and in Vitro Growth of *T. foetus* (ED₅₀) by the Top 10 Compounds from the Primary Library

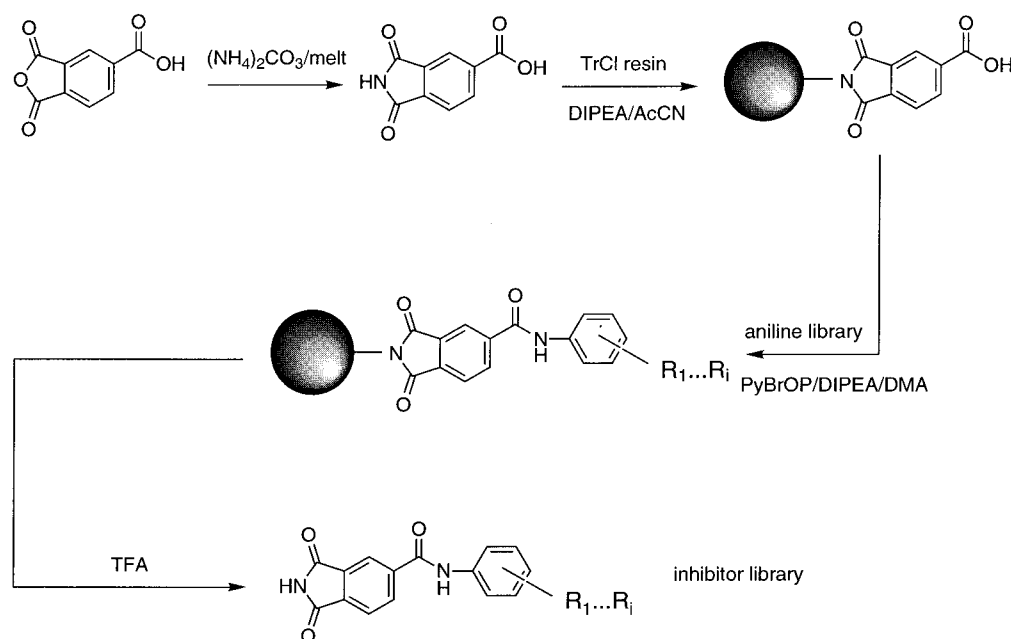
			
Cmpd ID	R	IC ₅₀ , μM	ED ₅₀ , μM
1		51	ND ^a
11		29	24
12		31	29
14		53	ND
15		33	39
16		27	58
20		16	19
23		36	ND
26		5	ND
28		43	ND
34		35	ND

^a Not determined.

H₅), 7.96 (d, 1, H_{6'}), 8.33 (d, 1, H_{5'}), 8.34 (s, 1, H_{3'}).

(4'-Phthalimidocarboxamido)-3-[(4-bromobenzyl)oxy]benzene (TF2): ¹H NMR (DMSO-*d*₆) δ 5.08 (s, 2, CH₂), 6.97–7.09 (2d, 2, H₅, H₆), 7.13 (d, 2, H₂', H_{6'}'), 7.40 (m, 3, H₃'', H₅'', H₄), 7.46 (d, 1, H₂), 7.92 (d, 1, H_{6'}), 8.30 (d, 1, H_{5'}), 8.31 (s, 1, H_{3'}).

Scheme 1



RESULTS AND DISCUSSION

Choice of Scaffold and Chemistry. Our first step in inhibitor design involved scaffold modification. A good choice of a scaffold (a) would lack any residual reactive functionalities, (b) would be easily amenable to combinatorial modification, preferably in a solid phase format, and (c) would not be associated with any known toxicities. Phthalimide appeared to fit all of these criteria. Nearly isosteric with phthalic anhydride, it presents an imide functionality that is suitable for attachment to the resin. A number of substituted phthalimides have been tested as potential medicinal candidates, and to our knowledge, they have not been associated with any specific kind of toxicity. In addition, the imide portion of the molecule mimics the C6–N1–C2 portion of xanthine, one of the natural substrates of HGXPRT. Since human HGXPRT does not act on xanthine, the phthalimide scaffold could potentially have built-in selectivity for the parasite enzyme.

To test our hypothesis, we prepared **1**, the phthalimide analogue of **TF1** (see below for discussion of the synthetic approach), and showed that it was equally active on HGXPRT as the parent compound **TF1** (Table 1). Since all of the previously described phthalic anhydride-based inhibitors of HGXPRT contained a conserved anilide moiety, we probed the possibility of introducing a flexible linker (between one and three methylene units) that would serve to attach the amide to the aromatic ring. None of the three compounds exhibited an appreciable inhibitory effect when tested on the HGXPRT (data not shown). Hence, we decided to prepare a library of phthalimidocarboxanilides in a search for selective HGXPRT inhibitors.

Primary Library Generation. The first step was to create a virtual library of anilines that are available for attachment to the phthalimide scaffold. Initial database mining was performed using the UC_Select program (18). It is a web-based CGI program which provides an interface for searching the Daylight version of the ACD database for compounds with desired structural features. The program also provides

for efficient Lipinski rule-based (23) elimination of compounds possessing undesirable structural features, i.e., filtering out the non-drug-like compounds by placing limits on molecular weight, lipophilicity, the number of charges, and hydrogen bond donors and acceptors. Optional extra SMILES arguments allow for additional customizable filtration protocols. In our case, the search resulted in a list of 873 anilines. Following removal of unreactive aminopurines and aminopyrimidines, the library was reduced to 750 entries. Visual inspection led to a further trimming of the library by removing anilines with three or more electron-withdrawing substituents, as well as di-ortho-substituted compounds, to a final size of 599 molecules.

The next step was to prepare the virtual phthalimidocarboxanilide library. An in-house program, UC_React (18), uses recursive SMARTS (19) to conduct user-defined chemistry *in silico*. It deletes atoms not present in the final product, and then joins the resulting fragments. This program was applied to the aniline collection mentioned earlier to produce a library of phthalimide derivatives with varying anilide chains. The resulting virtual library was used in docking experiments, and a final library of 32 reagents was eventually selected for synthesis (see Materials and Methods). Interestingly, the inhibitor containing the 3,4-dichloroanilide moiety that had been shown to be a micromolar inhibitor of HGXPRT was present consistently in the top 5% of DOCK scorers; it was subsequently removed from the final list of reagents.

A straightforward chemical scheme was implemented to access a variety of substituted phthalimidocarboxanilides (Scheme 1). Trimellitic anhydride, an exceptionally inexpensive starting material due to its broad application in polymer synthesis, was converted to 4-carboxyphthalimide at 280 °C using ammonium carbonate, and the scaffold was attached to the trityl chloride-functionalized resin. The resin served the dual purpose of providing support for solid phase synthesis and protecting the imide nitrogen. Coupling to the aniline library was carried out under standard conditions in

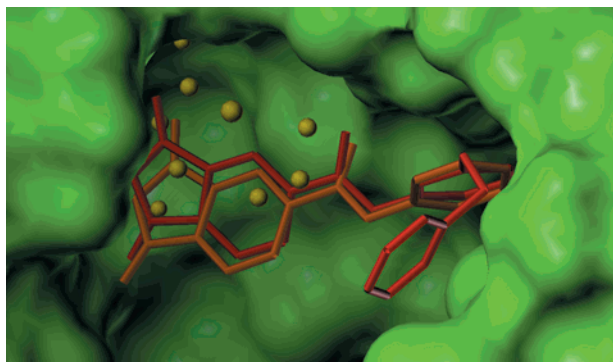


FIGURE 1: Modeled binding mode of **20** (red) in complex with *T. foetus* HGXPRT. Also shown are **TF1** (orange) and the sphere set used for docking (yellow). The modeled coordinates for **TF1** were taken from Somoza et al. (13); the nitro substituent is oriented away from the viewer. The larger sphere (corresponding to C2 of phthalimide) was used for chemical matching.

DIPEA/DMA. PyBrOP was found to give slightly better results than PyBOP, and was used throughout this study. To increase the coupling yields, the resin would typically be incubated at 37 °C for extended periods of time (5–7 days), with yields varying from 5 to 95%.

The synthesis of the primary 32-member library was carried out using standard parallel synthesis procedures, and the results for the top 10 compounds are shown in Table 1. They were all as good or better than the lead compound **1**. Most active substitutions were at the ortho and para positions in the anilide ring, with most compounds being between 2- and 10-fold more active than **1**. As mentioned earlier, 3,4-dichloroaniline was removed prior to the selection of the primary library. When it was added back to the library as a control, docking results placed it within the top 5% of scorers, significantly below the 15% threshold used in assembling the library. Hence, it is not surprising that most of the compounds in Table 1 displayed only modest improvements in their affinity for the enzyme over the initial lead **1**. The two best individual compounds were the derivatives of 3-aminophthalimide (**26**) and 3-(benzyloxy)aniline (**20**), with IC_{50} values of 5 and 16 μ M, respectively.

Phthalimide 20 as a Starting Point for the Secondary Library. In light of the activity data, the models could be re-evaluated in search of a reasonable secondary lead compound. Compound **20** appeared to be best suited for that role: (a) it was the second most potent member of the library, (b) the conformation originally proposed by DOCK was

similar to the minimized conformation of an unbound ligand, and (c) the benzyl ether linkage makes the compound easily amenable to further combinatorial exploration.

The model of the HGXPRT–**20** complex is shown in Figure 1. The phthalimide portion of the inhibitor appears to be slightly displaced from the position of the purine base. The anilide moiety is positioned between Thr 107 and Thr 110, implicated in binding the 5'-phosphate of GMP. The specificity for anilides at that position can be explained by the shallowness of the loop formed by residues 107–111, and the hydrophobic interactions of the aromatic ring of the anilide with the side chains of Leu 109 and Met 111. According to the model, the second aromatic ring attached to the anilide via the oxymethylene linker should also contribute the hydrophobic interactions with Leu 109. Unfortunately, the nine-residue loop from Tyr 74 to Asn 82, which has been shown to act as a flap that covers the catalytic pocket to shield the oxocarbenium transition state from nucleophilic attack by bulk solvent (24–26), is disordered in the X-ray structure of *T. foetus* HGXPRT, thus complicating the analysis of the contribution of this flexible loop to inhibitor binding. The carbonyl of Ser 73 is a mere 3.3 Å away from the face of the aromatic ring, underscoring the importance of that part of the protein in forming the binding pocket for **20**. The binding model for phthalimide inhibitor **20** closely resembles the previously published model of the *T. foetus* HGXPRT-bound phthalic anhydride-based inhibitor containing a 3-nitroanilide moiety (13) (Figure 1). The two models were obtained independently using different docking protocols (see Materials and Methods).

Effect of Substitutions in the Anilide Ring of 20. We initially chose to explore the binding pocket for the anilide moiety of **20**. Perturbations in this portion of **20** were modeled by redocking the modified inhibitors into the HGXPRT binding site. Small hydrophobic substitutions were slightly preferred at positions 2, 5, and 6 of the anilide ring, while no additional group could be accommodated at position 4. The directionality of the oxymethylene linker did not affect the docking score for analogues of compound **20**, which allowed for greater synthetic flexibility in the design of target molecules.

Three molecules, **20a–c**, were prepared using the solid phase format described earlier. The corresponding anilines were prepared using standard chemistry (Scheme 2) via reduction of the respective 3-substituted nitrobenzenes. As

Scheme 2

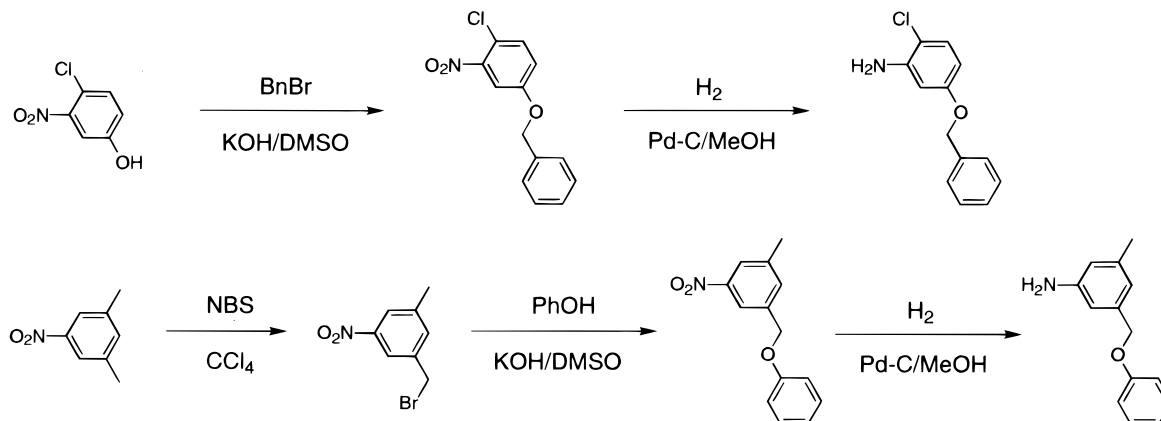
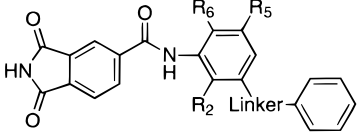


Table 2: Inhibition of *T. foetus* HGXPRT and in Vitro Growth of *T. foetus* by Derivatives of **20**


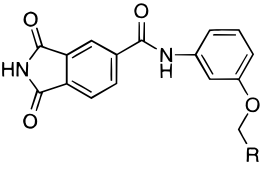
compd	linker	R ₂	R ₅	R ₆	IC ₅₀ (μM)	ED ₅₀ (μM)
20	O-CH ₂	H	H	H	16	19
20a	CH ₂ -O	H	Me	H	28	ND ^a
20b	O-CH ₂	H	H	Cl	8	ND
20c	O-CH ₂	Me	H	H	3	3.9

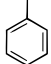
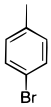
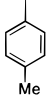
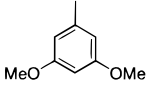
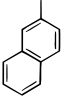
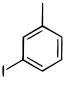
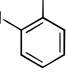
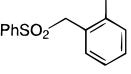
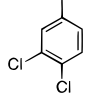
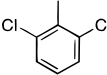
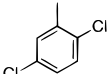
^a Not determined.

shown in Table 2, a chlorine at position 6 (**20b**), as well as the combination of a methyl at position 5 with the reversed methyleneoxy linker (**20a**), did not produce any appreciable improvement over **20**. Somewhat unexpectedly, introduction of the methyl substituent at position 2 led to a 5-fold increase in the extent of enzyme inhibition over the unmodified inhibitor. Since the substitution at that position would be expected to directly affect the conformation of the oxymethylene linker, a possible explanation for the observed increase in affinity of **20c** for HGXPRT could involve repositioning of the benzyloxy moiety within the enzyme's active site.

Synthesis of a Secondary Library. The second stage of our strategy involved optimization of the 3-benzyloxy substituent. Keeping the core intact, we decided to evaluate the effect of various substituents in the benzyl moiety on activity. The synthetic scheme involved introducing diversity at the first aniline-building step by alkylation of 3-nitrophenol with a variety of substituted benzyl bromides. Reduction of the nitroaromatics yielded a library of anilines that could be coupled to the resin to produce analogues of **20**.

Since the substituted benzyl derivatives of **20** would most likely interact with the flexible loop portion of HGXPRT which appears to be disordered in the X-ray structure (7), no preliminary requirements were placed on the starting benzyl bromide library. A search of available compounds that could be classified as benzyl bromide superstructures yielded 496 hits. After removal of undesirable functionalities (UC_Select), the search was narrowed to 63 entries, which were further filtered manually to the final group of 48 substituted benzyl bromides. By clustering these compounds with a complete-linkage hierarchical clustering program, we obtained 10 clusters and 11 singletons. Of these, 12 compounds were chosen by visual inspection as the representatives of various clusters so that they describe much of the geometric variability for mono- and disubstituted benzyl bromides. For 10 of the 12 compounds, sufficient amounts of the target phthalimidocarboxanilides were obtained, and their activity profile is shown in Table 3. Every compound in this secondary library produced an improvement over the lead **20**. The most active inhibitors were **20.1** (called **TF2** in the text) and **20.2**, bearing small hydrophobic substituents at the para position of the benzyl fragment, 4'-bromo and 4'-methyl, respectively. These inhibitors represented a 10-fold increase in the affinity for *T. foetus* HGXPRT compared to **20**. Compound **20.10**, having a 3'-chloro in addition to a

Table 3: Inhibition of *T. foetus* HGXPRT and in Vitro Growth of *T. foetus* by Analogues of **20** from the Secondary Library


Cmpd ID	R	IC ₅₀ , μM	ED ₅₀ , μM
20		16	19
20.1 (TF2)		1.5	2.8
20.2		1.7	ND ^a
20.3		8.2	ND
20.4		3.5	ND
20.5		8.9	ND
20.7		4.3	5.1
20.9		6.5	ND
20.10		3.5	4.6
20.11		12.1	ND
20.12		7.1	ND

^a Not determined.

4'-chloro substituent, appeared to be somewhat less potent, its IC₅₀ being nearly 5-fold lower than that of **20**.

According to the model, **TF2** would be expected to act as a competitive inhibitor of HGXPRT. Indeed, our experimental data indicated a competitive mode of inhibition by **TF2** with respect to guanine with a *K_i* of 0.49 ± 0.03 μM (Figure 2). We also noted an absence of competitive inhibition with respect to PRPP (data not shown), which

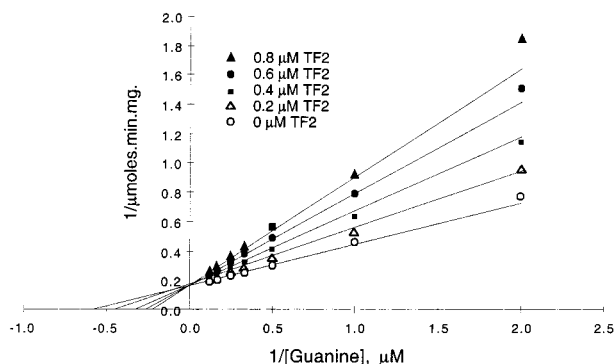


FIGURE 2: **TF2**-induced inhibition of *T. foetus* HGXPRT is competitive with guanine. The K_i value was determined to be $0.49 \pm 0.03 \mu\text{M}$.

Table 4: Inhibition of *T. foetus* HGXPRT by Derivatives of **20c**

Cmpd ID	R	IC ₅₀ , μM
20c		3
20c.1		5.2
20c.10		9.3

Table 5: Selective Inhibition of *T. foetus* HGXPRT by Derivatives of **20**

compd	IC ₅₀ (μM <i>T. foetus</i> HGXPRT)	IC ₅₀ (μM human HGXPRT)
20c	3	> 50 (82.4%) ^a
20.1	1.5	45
20.7	4.3	> 50 (88.3%)
20.10	3.5	24

^a Remaining enzyme activity at the stated inhibitor concentration.

would agree with the prediction of non-overlapping binding sites for **TF2** and PRPP.

Having found the best individual combinations for both the anilide and the benzyl moieties comprising inhibitor **20**, we combined the 2-methyl modification (**20c**) with substitutions at the 4'-position (**TF2** and **20.2**). Interestingly, the resulting inhibitors **20c.1** and **20c.10** were both less potent than all three parent compounds (Table 4). This finding indirectly supports our initial hypothesis, which holds that the 2-methyl substituent in **20c** induces a conformational change (most likely for the 3-benzyloxy group) which constitutes a departure from the conformations assumed by inhibitors **20**, **TF2**, and **20.2**.

Selective Inhibition of *T. foetus* HGXPRT. The most active phthalimidocarboxanilides were tested for inhibition of human HGXPRT (Table 5). All of the inhibitors were selective for *T. foetus* HGXPRT, but the extent of selectivity varied. Compounds **20c** and **20.7** were approximately 100-fold more selective; **TF2** was 30-fold more selective, and **20.10** displayed the lowest selectivity in this series (7x). It is tempting to speculate that the higher selectivity observed for

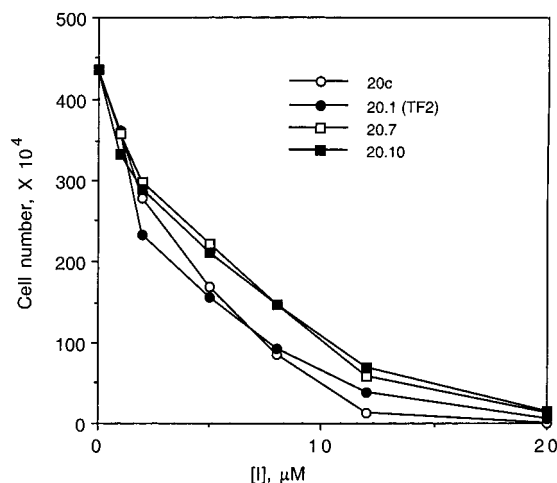


FIGURE 3: Concentration-dependent inhibition of *T. foetus* cell proliferation by HGXPRT inhibitors **20c**, **TF2**, **20.7**, and **20.10**.

the first two inhibitors is due to a similar conformation of the 3-benzyloxy substituent, as the 2'-iodo group in **20.7** may play a role similar to that of a 2-methyl group in creating steric hindrance between the face of the anilide and the 3-benzyloxy moiety.

Effects of HGXPRT Inhibitors on *T. foetus* Cell Culture. Having shown the competitive mode of HGXPRT inhibition by **TF2**, we explored the potential effect analogues of **20** may have on the growth of *T. foetus* cell culture. All of the inhibitors that were assayed were shown to be concentration-dependent inhibitors of *T. foetus* growth in culture, as shown in Figure 3 for the four most potent inhibitors. The ED₅₀ values are reported in Tables 1–3. Interestingly, the ED₅₀ values for all of the assayed phthalimidocarboxanilides, with the sole exception of **16**, were within 20% of their respective IC₅₀ values, serving as another indirect confirmation of the mode of action of these phthalimide derivatives. In the case of **16**, a 2-fold difference between ED₅₀ and IC₅₀ values was observed.

If the designed compounds act within the cells as competitive inhibitors of HGXPRT, addition of the substrate with which they are competing would be expected to reverse the growth inhibition (13). Indeed, **TF2**-induced inhibition of *T. foetus* growth can be reversed by increasing the concentration of hypoxanthine in the growth medium (Figure 4). A minimum hypoxanthine concentration between 0.2 and 0.5 mM ($K_M = 3 \mu\text{M}$ for *T. foetus* HGXPRT) was required for the survival of the cells challenged with $5 \mu\text{M}$ **TF2**. Hypoxanthine at concentrations of >1 mM essentially abolished any inhibition of cell proliferation under these experimental conditions.

Overall, the data being reported herein for a series of phthalimidocarboxanilides support the conclusion that these compounds inhibit growth of *T. foetus* parasite culture by selectively interfering with parasite purine salvage as inhibitors of the parasite's HGXPRT competitive with the purine substrate.

Utility of Functionalized Phthalimides as 6-Oxopurine Mimics. The compounds identified in the current study can be easily produced from inexpensive starting materials, a desirable feature of any potential antiparasitic agent. The molecules are sufficiently small (MW < 500) and lipophilic [clogP values vary in the 3.85–4.70 range for the most active

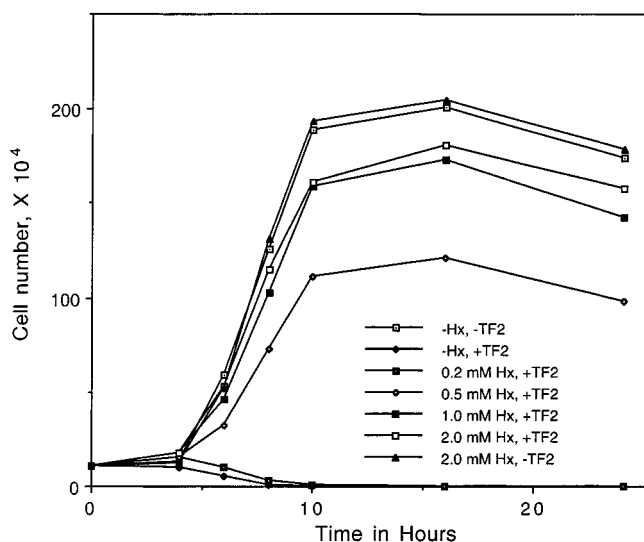


FIGURE 4: **TF2**-induced inhibition of *T. foetus* cell growth can be reversed by the addition of exogenous hypoxanthine. The concentration of **TF2** was kept at 5 μ M, while the amount of hypoxanthine added to the culture varied between 0 and 2 mM.

compounds as calculated using the *clogP* program (19)]; they contain two hydrogen bond donors and four hydrogen bond acceptors, thus satisfying Lipinski rules (23) for compounds best suited for passing through biological membranes.

Phthalimide could potentially serve as a general 6-oxopurine mimic for a variety of targets. We have identified micromolar phthalimide-based inhibitors for phosphoribosyltransferases with differing specificities, including human HGPR and *Giardia lamblia* GPRT; in each case, the anilide portion of the active inhibitor was drastically different (data not shown). We believe that it might be possible to use this scaffold as a 6-oxopurine mimic and tailor the "side chain" portion of the inhibitor on the basis of the X-ray structure of the target.

CONCLUSION

We have used a previously reported phthalic anhydride scaffold to identify novel inhibitors of *T. foetus* HGXPRT. Conversion of the scaffold to phthalimide produced biologically stable molecules. A round of structure-based combinatorial library design coupled with solid phase parallel synthesis produced low-micromolar inhibitors of the parasite enzyme. Further combinatorial exploration of a select secondary lead compound led to identification of several biologically active submicromolar inhibitors of *T. foetus* HGXPRT. Our findings demonstrate the success of a structure-based computational approach to drug design, whereby a molecule identified by computer-based means can be rationally modified to produce potent inhibitors of a chosen target enzyme. The approach described herein could

prove to be useful in rapid development of inhibitors for a number of targets possessing 6-oxopurine binding sites.

ACKNOWLEDGMENT

We thank Drs. A. Geoffrey Skillman, Jr., and Connie M. Oshiro for their insights and thoughtful discussions. We are also grateful to Ms. Anne Sarver for her assistance in performing the assays of human HGPR.

REFERENCES

- Hunter, W. H. (1997) *Parasitology* 114, S17–S29.
- Gutteridge, W. E. (1997) *Parasitology* 114, S145–S151.
- Haque, T. S., Skillman, A. G., Lee, C. E., Habashita, H., Gluzman, I. Y., Ewing, T. J. A., Goldberg, D. E., Kuntz, I. D., and Ellman, J. A. (1999) *J. Med. Chem.* 42, 1428–1440.
- Wang, C. C. (1984) *J. Med. Chem.* 27, 1–9.
- Wang, C. C. (1997) *Parasitology* 114, S31–S44.
- Wang, C. C., Verham, R., Rice, A., and Tzeng, S. F. (1983) *Mol. Biochem. Parasitol.* 8, 325–337.
- Somoza, J. R., Chin, M. S., Focia, P. J., Wang, C. C., and Fletterick, R. J. (1996) *Biochemistry* 35, 7032–7040.
- Kuntz, I. D., Blaney, J. M., Oatley, S. J., Langridge, R., and Ferrin, T. (1982) *J. Mol. Biol.* 161, 269–288.
- Meng, E. C., Shoichet, B. K., and Kuntz, I. D. (1992) *J. Comput. Chem.* 13, 505–524.
- Meng, E. C., Gschwend, D. A., Blaney, J. M., and Kuntz, I. D. (1993) *Proteins: Struct., Funct., Genet.* 17, 268–278.
- Ewing, T. J. A., and Kuntz, I. D. (1997) *J. Comput. Chem.* 18, 1175–1189.
- Available Chemicals Directory, version 98.2 (1998) Molecular Design Limited Information Systems, San Leandro, CA.
- Somoza, J. R., Skillman, A. G., Jr., Munagala, N. R., Oshiro, C. M., Knettel, R. M. A., Mpoke, S., Fletterick, R. J., Kuntz, I. D., and Wang, C. C. (1998) *Biochemistry* 37, 5344–5348.
- Chin, M. S., and Wang, C. C. (1994) *Mol. Biochem. Parasitol.* 63, 221–229.
- Eads, J. C., Scapin, G., Xu, Y., Grubmeyer, C., and Sacchettini, J. C. (1994) *Cell* 78, 325–334.
- Sybyl, version 6.5 (1999) Tripos Associates, St. Louis, MO.
- Insight II, version 98.0 (1998) Molecular Simulations, Inc., San Diego, CA.
- Skillman, A. G., and Kuntz, I. D., unpublished results.
- Daylight, version 4.61 (1997) Daylight Chemical Information Systems, Inc., Santa Fe, NM.
- Kanaaneh, J., Craig, S. P., III, and Wang, C. C. (1994) *Eur. J. Biochem.* 223, 595–601.
- Yuan, L., Craig, S. P., McKerrow, J. H., and Wang, C. C. (1992) *Biochemistry* 31, 806–810.
- Aronov, A. M., and Gelb, M. H. (1998) *Tetrahedron Lett.* 39, 4947–4950.
- Lipinski, C. A., Lombardo, F., Dominy, B. W., and Feeney, P. J. (1997) *Adv. Drug Delivery Rev.* 23, 3–25.
- Schumacher, M. A., Carter, D., Roos, D. S., Ullman, B., and Brennan, R. G. (1996) *Nat. Struct. Biol.* 3, 881–887.
- Shi, W., Li, C. M., Tyler, P. C., Furneaux, R. H., Grubmeyer, C., Schramm, V. L., and Almo, S. C. (1999) *Nat. Struct. Biol.* 6, 588–593.
- Shi, W., Li, C. M., Tyler, P. C., Furneaux, R. H., Cahill, S. M., Girvin, M. E., Grubmeyer, C., Schramm, V. L., and Almo, S. C. (1999) *Biochemistry* 38, 9872–9880.

BI992555G